General Disclaimer

One or more of the Following Statements may affect this Document

- This document has been reproduced from the best copy furnished by the organizational source. It is being released in the interest of making available as much information as possible.

- This document may contain data, which exceeds the sheet parameters. It was furnished in this condition by the organizational source and is the best copy available.

- This document may contain tone-on-tone or color graphs, charts and/or pictures, which have been reproduced in black and white.

- This document is paginated as submitted by the original source.

- Portions of this document are not fully legible due to the historical nature of some of the material. However, it is the best reproduction available from the original submission.

OLD DOMINION UNIVERSITY RESEARCH FOUNDATION

DEPARTMENT OF PHYSICS AND GEOPHYSICAL SCIENCES
SCHOOL OF SCIENCES AND HEALTH PROFESSIONS
OLD DOMINION UNIVERSITY
NORFOLK, VIRGINIA

Technical Report PGSTR-PH76-45

ANALYTICAL STUDY OF THE OPTIMUM GEOMETRIC CONFIGURATION OF A SPACE SHUTTLE MATERIALS LABORATORY

By

Forrest P. Clay, Jr.

and

J.E. Heuser

Final Report

Prepared for the
National Aeronautics and Space Administration
Langley Research Center
Hampton, Virginia

Under
Research Grant NGR 47-003-082
April 1, 1973 - June 30, 1976
Leonard T. Melfi, Technical Monitor
Space Systems Division

December 1976

DEPARTMENT OF PHYSICS AND GEOPHYSICAL SCIENCES
SCHOOL OF SCIENCES AND HEALTH PROFESSIONS
OLD DOMINION UNIVERSITY
NORFOLK, VIRGINIA

Technical Report PGSTR-PH76-45

ANALYTICAL STUDY OF THE OPTIMUM GEOMETRIC CONFIGURATION OF A SPACE SHUTTLE MATERIALS LABORATORY

By

Forrest P. Clay, Jr.

and

J.E. Hueser

Final Report

Prepared for the
National Aeronautics and Space Administration
Langley Research Center
Hampton, Virginia 23665

Under
Research Grant NGR 47-003-082
April 1, 1973 - June 30, 1976
Leonard T. Melfi, Technical Monitor
Space Systems Division

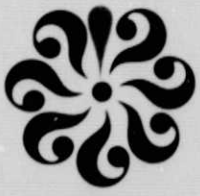

Submitted by the
Old Dominion University Research Foundation
Norfolk, Virginia 23508

December 1976

ANALYTICAL STUDY OF THE OPTIMUM GEOMETRIC CONFIGURATION OF A SPACE SHUTTLE MATERIALS LABORATORY

By

Forrest P. Clay, Jr. and J.E. Hueser

INTRODUCTION

This final report indicates the extent to which the specific tasks outlined in the original grant (NGR 47-003-082) and the subsequent continuations have been addressed. Each of the tasks have either been completed with documentation in the form of published journal articles and oral presentations, indicated in the list of publications, or have been partially completed with additional proposed effort continued in a subsequent grant (NSG 1271).

FEASIBILITY STUDY OF THE MOLECULAR SHIELD

The theoretical analysis of the feasibility of the molecular shield concept has been completed. It was concluded that there are no inherent physical constraints which prohibit attaining a background density inside the molecular shield of less than 10^3 cm^{-3} for the projected range of Shuttle orbit heights (publs. 1 and 2). A model has been proposed to evaluate the effects of the relative size and relative outgassing rate of anticipated experiments (publ. 3)(see Appendix I).

Experimental apparatus is being assembled to evaluate the desorption characteristics of several potential shield construction materials and to determine the necessary processing required to reduce the outgassing rate of both the shield and experimental hardware prior to launch.

A Monte Carlo program has been developed and is presently being used to evaluate the effects of Shuttle related sources on the density in the vicinity of and inside the shield.

DESIGN, DEVELOPMENT, AND EXPERIMENTAL EVALUATION OF QUADRUPOLE MASS SPECTROMETER CIRCUITS

The design and development of flight prototype circuits for analytical instrumentation to be used in conjunction with the molecular shield was initiated or continued under grant NGR 47-003-082 and is presently being funded under grant NSG 1271.

The areas of highest priority were determined to be circuits for the following mass spectrometer functions:

a. Ion source voltage supplies

b. Quadrupole excitation circuits

c. Mass line reference voltage supplies

d. Mass line selection circuits

e. Ion counting circuits.

As significant advances were made the results were documented (publs. 4 through 7). A detailed description of the present status is presented in Appendix II.

PARTIAL LIST OF PUBLICATIONS GENERATED UNDER THIS GRANT

1. Melfi, Leonard T.; R.A. Outlaw; and F.J. Brock: "Molecular shield: An orbiting low-density materials laboratory." J. Vac. Sci. Technol., 13, 698, May/June 1976.

2. Hueser, J.E.; and F.J. Brock: "Theoretical analysis of the density within an orbiting molecular shield." J. Vac. Sci. Technol., 13, 702, May/June 1976.

3. Hueser, J.E.,; S.K. Park; and F.J. Brock: "The effect of experiments on the density distribution in a molecular shield." To be published, see Appendix I.

4. Clay, F.P., Jr.; F.J. Brock; and L.T. Melfi, Jr.: "The emission efficiency of a hot filament in the presence of O_2 at various pressures and techniques for maintaining constant emission." Published abstract, Virginia J. of Sci., 24, No. 3, Fall 1973.

5. Clay, Forrest P., Jr.; F.J. Brock; and Leonard T. Melfi, Jr.: "Switching regulator emission control circuit for ion sources." Rev. Sci. Instrum., 46, 528, 1975.

6. Clay, F.P., Jr.; L.T. Melfi, Jr.; and F.J. Brock: "Evaluation of a thoria coated iridium cathode for an ion source." Published abstract, Virginia J. of Sci., 26, No. 2, Summer 1975.

7. F.P. Clay, Jr.: "Circuit innovations associated with the design of a flyable quadrupole mass spectrometer." Published abstract, Program of 43rd Annual Meeting of SESAPS, November 1976.

APPENDIX I

THE EFFECT OF EXPERIMENTS ON THE DENSITY DISTRIBUTION IN A MOLECULAR SHIELD*

J.E. Hueser[1], S.K. Park[2], and F.J. Brock[1]

[1] Department of Physics and Geophysical Sciences, Old Dominion University, Norfolk, Virginia 23508.

[2] Analysis and Computation Division, NASA Langley Research Center, Hampton, Virginia 23665.

ABSTRACT

A steady state, collisionless flow analysis has been made of the density distribution within a hemisphere-disc system due to independent, uniformly distributed internal gas sources. The model may be used to estimate the density within a molecular shield, deployed from the Shuttle Orbiter, which contains internal experiments having a prescribed gas source. Contour plots of the density distribution within the system are presented for disc-to-hemisphere radius ratios of .1, .3, .5, .7, and for disc-to-hemisphere surface emission flux density ratios of .01, 1, 100. The hemisphere-disc system is compared to the empty hemisphere and it is found that if the disc emission flux density is the same as the hemisphere and the disc radius is not greater than 1/3 of the hemisphere radius, the increase in density at the center of the hemisphere-disc system is less than 50%.

INTRODUCTION

There are experiments planned for the Shuttle Orbiter which require a very low background gas density. It has been shown that this condition can be satisfied in a molecular shield deployed from the orbiter[1,2] within which the density due to all atmospheric species is less than 10^3 cm^{-3}. However, there are some experiments which have intrinsic gas sources associated with outgassing of the apparatus, sample, etc., and some experiments which release gases internally during the experiment. In this class of experiments, it is probable that the gas density within the molecular shield is principally due to the internal gas sources.

An estimate may be made of the molecular density distribution within the molecular shield for this class of experiments by analyzing the density distribution in a geometric model with adjustable parameters which can be chosen to represent the important properties of the molecular shield with an experiment installed. For present purposes, these properties are: (1) the magnitude of the gas source associated with the experiment, and (2) the mean probability of molecular escape through the channel between the experiment and the molecular shield. It is the purpose of this paper to analyze the internal density distribution for a model which is geometrically similar to the molecular shield and which has two independently adjustable parameters.

MODEL

An analytically amenable model which consists of a hemispherical shell of radius R_o and a disc of radius R_i is shown in Fig. 1. A uniform source flux density ν^o, corresponding to surface outgassing originates at the surface of the hemisphere, and a uniform source flux density ν^i, corresponding to the experiment gas source originates at the surface of the disc. Both ν^o and ν^i are assumed to be in thermal equilibrium with the isothermal surfaces of the model and to have a cosine angular distribution with respect to the local surface normal. Suppose the experiment gas source is $\dot{N}$ (the number of molecules leaving the experiment per unit time), then the model is matched to the experiment by setting $\dot{N} = \pi R_i^2 \nu^i$ and adjusting the annular

area $\pi(R_o^2 - R_i^2)$ to approximate the molecular escape probability of the molecules released by the experiment.

ANALYSIS

The calculation of the molecular density within the model first requires the calculation of the emission flux density distribution for each surface. At a disc surface increment ds_i (see Fig. 2), there is an incident flux density ν_i, consisting of molecules emitted from surface elements of the hemisphere ds_o, in a direction such that they can reach ds_i. Particle conservation at ds_i requires that the emission flux density ν_e equals the sum of the incident flux density ν_i and the flux density ν^i which originates at ds_i, that is

$$\nu_i + \nu^i = \nu_e \quad . \tag{1}$$

Under the assumption that the angular dependence of the emission flux density is given by a cosine function, the flux density emitted by a surface element must satisfy the relation

$$\nu_e = \int_\Omega I\cos\gamma d\omega \quad , \tag{2}$$

where $I\cos\gamma$ is the emission flux density per unit solid angle, γ is the angle between the surface normal and $d\omega$, and Ω indicates that the integration extends over the half-space solid angle into which all molecules are emitted. From symmetry it is clear that I is independent of the azimuthal coordinate. It follows that

$$\nu_e = \pi I \quad . \tag{3}$$

The incremental flux density $d\nu_i$ incident on ds_i emitted from ds_o must satisfy the relation

$$d\nu_i ds_i = I^o \cos\gamma_o d\omega_o ds_o \quad , \tag{4}$$

and from Fig. 2 it follows that

$$d\omega_o = \cos\gamma_i ds_i/\rho^2 \quad . \tag{5}$$

Substituting Eq. (5) into Eq. (4), integrating over ds_o, then substituting this result and Eq. (3) into Eq. (1) gives

$$\pi I^i = \nu^i + \int_\Sigma I^o \cos\gamma_o \cos\gamma_i ds_o/\rho^2 \quad , \tag{6}$$

where Σ indicates that the integration extends over the surface of the hemisphere. From Fig. 2 it follows that

$$\cos\gamma_o \cos\gamma_i ds_o/\rho^2 = (1 - \hbar\sin\theta\cos\phi)\{1 - 2\hbar\sin\theta\cos\phi + \hbar^2\}^{-2} \sin\theta\cos\theta\, d\theta d\phi \quad . \tag{7}$$

Substituting Eq. (7) into Eq. (6) and recalling that I^o is independent of ϕ, the integration over ϕ may be performed[3] and Eq. (6) may then be written

$$I^i(\hbar) = \nu^i/\pi + 2\int_0^{\pi/2} I^o(\theta)(1 + \hbar^2\cos 2\theta)\{1 + 2\hbar^2\cos 2\theta + \hbar^4\}^{-3/2} \cos\theta\sin\theta\, d\theta \quad , \tag{8}$$

$$(0 \leq \hbar \leq \hbar') \quad .$$

At a hemisphere surface element ds_o (see Fig. 3), there is an incident flux density ν_{io} of molecules emitted by all surface elements ds_o' in a direction such that they can reach ds_o, and an incident flux density ν_{ii} of molecules emitted from all surface elements ds_i of the disc in a direction such that they can reach ds_o. There is also a source flux density ν^o leaving ds_o. Particle conservation at ds_o requires that the sum of these flux densities be equal to the emission flux density from ds_o, thus

$$\nu_{io} + \nu_{ii} + \nu^o = \pi I^o \quad , \tag{9}$$

where Eq. (3) has been used to eliminate ν_e in terms of I^o. The flux incident on ds_o emitted from ds_o' must satisfy the relation

$$d\nu_{io} ds_o = I^o \cos\gamma_o' ds_o' d\omega' \quad , \tag{10}$$

where from Fig. 3 it follows that

$$d\omega' = \cos\gamma_o ds_o/\rho^2 \tag{11}$$

and

$$ds_o'/R_o^2 = \sin\theta'\, d\theta'\, d\phi_o \quad . \tag{12}$$

Since both ds_o and ds_o' are on the surface of the hemisphere, it follows that

$$R_o^2 \cos\gamma_o \cos\gamma_o'/\rho^2 = 1/4 \quad . \tag{13}$$

Similarly, the flux incident on ds_o emitted from ds_i is given by

$$d\nu_{ii} ds_o = I^i \cos\gamma_i ds_i d\omega_i \quad , \tag{14}$$

and from Fig. 3 it may be seen that

$$d\omega_i = \cos\bar{\gamma} ds_o/\lambda^2 \quad . \tag{15}$$

Substituting Eqs. (11) and (13) into Eq. (10) and integrating over the surface of the hemisphere; substituting Eq. (15) into (14) and integrating over the surface of the disc; and then substituting these results into Eq. (9) yields

$$\pi I^o = \nu^o + (4R_o^2)^{-1} \int_\Sigma I^o ds_o' + \int_\sigma I^o \cos\gamma_i \cos\bar{\gamma} ds_i/\lambda^2 \quad , \tag{16}$$

where Σ indicates that integration is over the surface of the hemisphere and σ indicates that integration is over the surface of the disc. From Fig. 3 it may be seen that

$$\cos\gamma_i \cos\bar{\gamma} ds_i/\lambda^2 = (1 - r\sin\theta\cos\theta_i)\{1 - 2r\sin\theta\cos\phi_i + r^2\}^{-2} \cos\theta\, r dr d\phi_i \quad . \tag{17}$$

Substituting Eqs. (12) and (17) into Eq. (16) and recalling that the functions I^o and I^i are independent of the azimuthal angles, the ϕ_i and ϕ_o integrations may be performed[3] and Eq. (16) may then be written

$$I^o(\theta) = \nu^o/\pi + \frac{1}{2}\int_o^{\pi/2} I^o(\theta)\sin\theta\, d\theta + 2\int_o^{r'} I^i(r)(1 + r^2\cos 2\theta)\{1 + 2r^2\cos 2\theta + r^4\}^{-3/2} \cos\theta\, r dr \quad , \quad (0 \le \theta \le \pi/2) \quad , \tag{18}$$

where the prime on θ in the first integral has been dropped since it is a definite integral, and r' is the disc radius normalized by R_o.

Eqs. (8) and (18) are a coupled set of integral equations, the solutions of which yield the functions $I^i(r)$ and $I^o(\theta)$. It is convenient to write these equations in dimensionless form by applying the following set of transformation equations (which also remove their explicit dependence on the emission flux densities):

$$\left.\begin{aligned} J^i(r) &= \pi I^i(r)/(\nu^i + 2\nu^o) \\ J^o(\theta) &= \pi I^o(\theta)/(\nu^i + 2\nu^o) - \{1 + \nu^i/(2\nu^o)\}^{-1} \end{aligned}\right\} \tag{19}$$

Eq. (8) may then be written

$$J^i(r) = 1 + 2\int_o^{\pi/2} J^o(\theta) g(r,\theta) \sin\theta\, d\theta \quad , \quad (0 \le r \le r') \tag{20}$$

and Eq. (18) may be written

$$J^o(\theta) = \frac{1}{2}\int_o^{\pi/2} J^o(\theta)\sin\theta\, d\theta + 2\int_o^{r'} J^i(r) g(r,\theta) r dr \quad , \quad (0 \le \theta \le \pi/2) \quad , \tag{21}$$

where

$$g(r,\theta) = (1 + r^2\cos 2\theta)\{1 + 2r^2\cos 2\theta + r^4\}^{-3/2} \cos\theta \quad . \tag{22}$$

Appendix A gives an outline of the numerical method used to solve Eqs. (20) and (21). Solutions of $J^i(r)$ and $J^o(\theta)$ are presented in Fig. 4 for values of the system parameter $r' = .1, .3, .5, .7$.

Having determined the emission functions $I^i(r)$ and $I^o(\theta)$ it is now possible to determine the density distribution within the hemisphere. The molecular density at a distance ρ (see Fig. 5) from an emitting surface element is given by

$$dn(\rho) = \sqrt{\pi}(2v_m)^{-1} d\nu(\rho) \tag{23}$$

where $v_m = (2kT/m)^{1/2}$. Continuity of flux at the point ρ requires that

$$d\nu(\rho)ds = d\nu_e ds_e \quad , \tag{24}$$

and from Fig. 5, $ds = \rho^2 d\omega_e$. Assuming that the emission flux angular distribution has a cosine dependence, the incremental emission flux in the direction γ_e is given by

$$d\nu_e = I \cos\gamma_e \, d\omega_e \quad . \tag{25}$$

Eq. (23) may then be written

$$dn(\rho) = \sqrt{\pi}(2v_m)^{-1} I \cos\gamma_e \, ds_e/\rho^2 \quad . \tag{26}$$

Applying Eq. (26) to the emission functions $I^i(r)$ and $I^o(\theta)$, the density at a point (ρ,μ) within the hemisphere (see Fig. 6) is given by

$$n(\rho,\mu) = \sqrt{\pi}(2v_m)^{-1} \left\{ \int_\Sigma I^o(\theta)\cos\gamma_o \, ds_o/\rho_o^2 + \int_\sigma I^i(r)\cos\gamma_i \, ds_i/\rho_i^2 \right\} \quad , \tag{27}$$

where Σ indicates integration over the surface of the hemisphere and σ indicates integration over the surface of the disc. From Fig. 6 it follows that

$$\cos\gamma_o ds_o/\rho_o^2 = \{1 - \rho(\sin\mu\sin\theta\cos\phi_o + \cos\mu\cos\theta)\}\{1 - 2\rho(\sin\mu\sin\theta\cos\phi_o + \cos\mu\cos\theta) + \rho^2\}^{-3/2} \sin\theta d\theta d\phi_o \tag{28}$$

and

$$\cos\gamma_i ds_i/\rho_i^2 = \rho\cos\mu\{\rho^2 - 2\rho r\sin\cos\phi_i + r^2\}^{-3/2} r dr d\phi_i \quad . \tag{29}$$

Substituting Eqs. (28) and (29) into Eq. (27) and using the transformation Eqs. (19) and then performing the integrations over ϕ_i and ϕ_o[3], yields the normalized density distribution within the hemisphere

$$\bar{n}(\rho,\mu) = 2\rho\cos\mu \int_0^{\lambda'} J^i(\lambda) f_1(\rho,\mu,\lambda)\lambda d\lambda + \int_0^{\pi/2} J^o(\theta) f_2(\rho,\mu,\theta)\sin\theta d\theta + \{1 + \nu^i/(2\nu^o)\}^{-1} \int_0^{\pi/2} f_2(\rho,\mu,\theta)\sin\theta d\theta \quad , \tag{30}$$

where the normalization relation is given by

$$n(\rho,\mu) = (\nu^i + 2\nu^o)\bar{n}(\rho,\mu)/(\sqrt{\pi}v_m) \quad , \tag{31}$$

and where

$$f_1(\rho,\mu,\lambda) = E(q_1)\{\lambda^2 - 2\lambda\rho\sin\mu + \rho^2\}^{-1}\{\lambda^2 + 2\lambda\rho\sin\mu + \rho^2\}^{-1/2} \tag{32}$$

and

$$f_2(\rho,\mu,\theta) = \{(1 - \rho^2)E(q_2)(1 - 2\rho\cos(\theta - \mu) + \rho^2)^{-1} + K(q_2)\}(1 - 2\rho\cos(\theta + \mu) + \rho^2)^{-1/2} \tag{33}$$

and where $K(q)$ is a complete elliptic integral of the 1st kind, $E(q)$ is a complete elliptic integral of the 2nd kind[3], and the moduli are given by

$$q_1^2 = 4\lambda\rho\sin\mu(\lambda^2 + 2\lambda\rho\sin\mu + \rho^2)^{-1} \quad , \tag{34}$$

$$q_2^2 = 4\rho\sin\mu\sin\theta(1 - 2\rho\cos(\theta + \mu) + \rho^2)^{-1} \quad . \tag{35}$$

Eq. (30) has been solved numerically for ρ = .01(.01).99 and μ = 0.0(2)80, 81(1)85, 85.1(.1)89.9 degrees. Solutions were generated for values of the system parameters: λ' = .1(.1).9 and ν^i/ν^o = .01, .1, 1, 10, 100. Plots of constant density contours within the model are presented in Fig. 7 for the system parameters λ' = .1, .3, .5, .7 and ν^i/ν^o = .01, 1, 100. These curves are normalized with respect to the density (normalized) at the origin, the value of which is written on each figure. Thus the normalized density at any point (ρ,μ) is the produced of the contour parameter and $\bar{n}(0,0)$. Inserting this product into Eq. (31) yields the molecular number density at the point (ρ,μ).

DISCUSSION

The hemisphere-disc system is compared to the empty hemisphere in Fig. 8 (using data taken from ref. 2 for the empty hemisphere). The ordinate is the density at the center of the hemisphere-disc system ($\rho = 1/2$, $\mu = 0$) divided by the density in the empty hemisphere at the same point. The abscissa is the normalized disc radius, $\hbar'$. Curves are presented for emission flux density ratios $\nu^i/\nu^o = .01, 1, 100$. Since $\nu^i/\nu^o = .01$ implies that the disc gas source is negligible compared to the hemisphere, the lower curve may be interpreted (approximately) as the increase in density due to the reduction in molecular escape probablity by the disc. The upper curve illustrates the rapid increase in density if the total gas source is dominated by the disc ($\nu^i/\nu^o = 100$) even for a relatively small disc radius.

To minimize the density within the molecular shield during flight, the radius of the shield should be large with respect to an experiment installed within the shield and the experiment apparatus should be thoroughly degassed. Assuming that the shield radius is approximately a factor of 3 larger than the mean radius of an installed experiment and that the experiment outgassing rate is approximately the same as the shield outgassing rate (since both would have experienced the same degassing treatment prior to flight), the density within the shield-experiment system may be estimated by evaluating the density within the hemisphere-disc model. Under these assumptions the model parameters have the values $\hbar' = 1/3$ and $\nu^i/\nu^o = 1$. A typical value for the outgassing rate of a thoroughly degassed metal is $\nu = 3 \times 10^7$ cm^{-2} sec^{-1} (molecular hydrogen). From Eq. (31), for a temperature of 300 K, and the data shown in Fig. 7e, the density at the center of the system ($\rho = 1/2$, $\mu = 0$) is $n(1/2, 0) = 1293$ cm^{-3}. This may be compared with a density of 974 cm^{-3} at the same point in an empty hemisphere[2]. Thus inserting an experiment not exceeding 1/3 the size of the hemisphere and having an equal outgassing rate increases the density at the center of the system less than 50%.

APPENDIX A

The coupled integral equations, Eqs. (20) and (21), may be solved simultaneously by the method outlined below. Let:

$$y_i = J^i(r_i) \quad , \tag{A1}$$

$$x_j = J^o(\theta_j) \quad , \tag{A2}$$

$$r_i = \frac{i}{m} r' \quad , \quad i = 0, 1, 2, 3, \ldots m \quad , \tag{A3}$$

$$\theta_j = \frac{j}{n} \frac{\pi}{2} \quad , \quad j = 0, 1, 2, 3, \ldots n \quad , \tag{A4}$$

$$K_{ij} = \frac{(1 + r_i^2 \cos 2\theta_j)\cos\theta_j}{[1 + 2r_i^2 \cos 2\theta_j + r_i^4]^{3/2}} = g(r_i, \theta_j) \quad . \tag{A5}$$

Then Eqs. (20) and (21) may be written in discretized form (where the w's are the weighting factors of the integration formula used)

$$y_i = 1 + (\pi/n) \sum_{j=1}^{n} K_{ij} w_j x_j \sin\theta_j \quad , \quad i = 1, 2, 3, \ldots m \quad , \tag{A6}$$

$$x_j = \pi(4n)^{-1} \sum_{k=1}^{n} w_k x_k \sin\theta_k + 2(r'/m) \sum_{i=1}^{m} K_{ij} w_i r_i y_i \quad , \quad j = 1, 2, 3, \ldots n \quad , \tag{A7}$$

with the ancillary equations

$$y_0 = 1 + (\pi/n) \sum_{j=1}^{n} K_{0j} w_j x_j \sin\theta_j \tag{A8}$$

$$x_0 = \pi(4n)^{-1} \sum_{k=1}^{n} w_k x_k \sin\theta_k + 2(r'/m) \sum_{i=1}^{m} K_{i0} w_i r_i y_i \quad . \tag{A9}$$

Using matrix notation Eqs. (A6) and (A7) may be written

$$Y = L_m + (\pi/n) K W_n S X \tag{A10}$$

$$X = \pi(4n)^{-1} L_n L_n^T W_n S X + 2(r'/m) K^T W_m R Y \quad , \tag{A11}$$

where L_m, L_n are column vectors of length m,n with all elements equal to 1, K is an $m \times n$ matrix with elements K_{ij}, W_m, W_n, S and R are diagonal matrices

with elements w_i, w_j, $\sin\theta_j$, and r_i respectively, Y, X are column vectors of length m, n with elements y_i, x_j respectively, and $(\cdot)^T$ denotes transpose.

Eliminating Y in Eqs. (A10) and (A11) yields

$$Ax = B \quad , \tag{A12}$$

where

$$A = I_n - \pi(4n)^{-1} L_n L_n^T W_n S - 2\pi r'(mn)^{-1} K^T W_m R K W_n S \quad , \tag{A13}$$

$$B = (2r'/m) K^T W_m R L_m \quad , \tag{A14}$$

and I_n is the $n \times m$ identity matrix. Solving Eq. (A12) for X and substituting the results of Eq. (A10) yields the solution for Y and substituting these results into Eqs. (A8) and (A9) gives x_0 and y_0.

Numerical experimentation revealed that with n = 100 and m = r'n this method produces X and Y solutions with a relative error $< 10^{-6}$ for the full range of (r,θ) and $r' \leq .7$. The weights w_i were chosen by Simpson's rule.

REFERENCES

1) L.T. Melfi, Jr., R.A. Outlaw, J.E. Hueser, and F.J. Brock, J. Vac. Sci. Technol. 13, 698 (1976).

2) J.E. Hueser, and F.J. Brock, J. Vac. Sci. Technol. 13, 702 (1976).

3) I.S. Gradshteyn, and I.M. Ryzhik, Tables of Integrals Series and Products (Academic Press, New York, 1965).

* Work supported by NASA grants NGR 47-003-043, NGR 47-003-082, and NSG 1271 through the Old Dominion University Research Foundation.

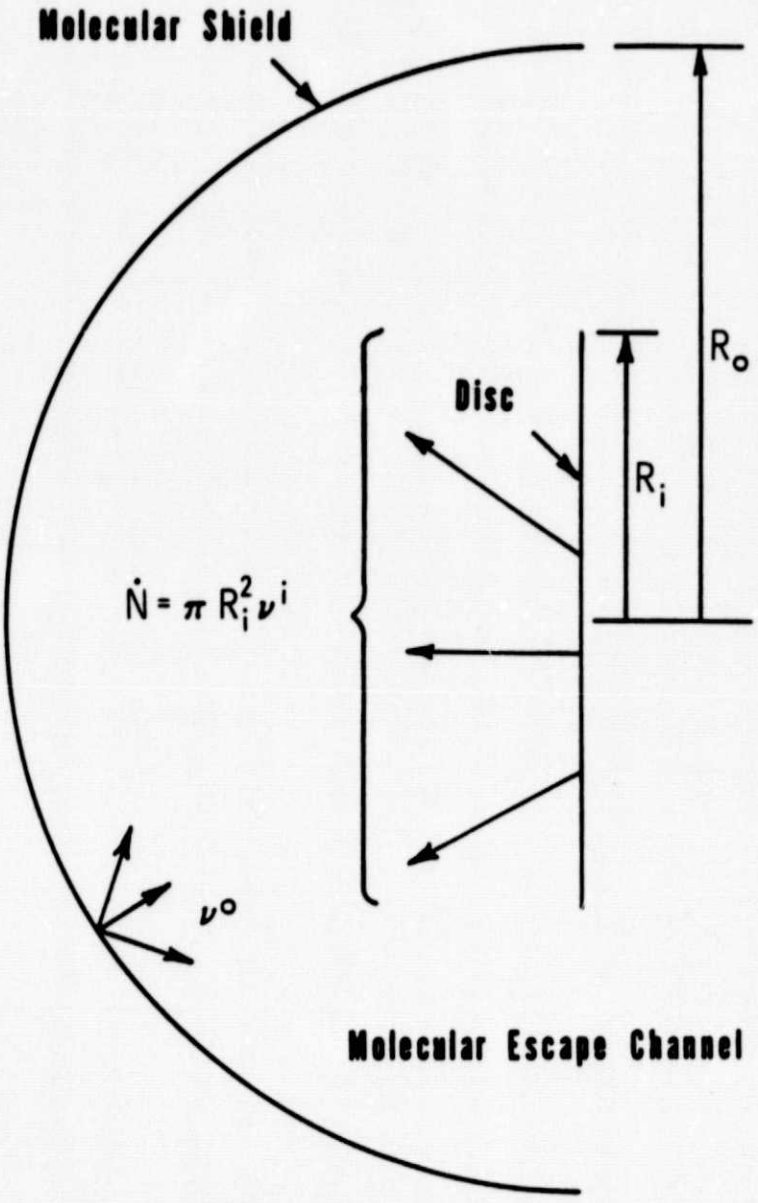

Figure 1. Schematic representation of the hemisphere-disc model.

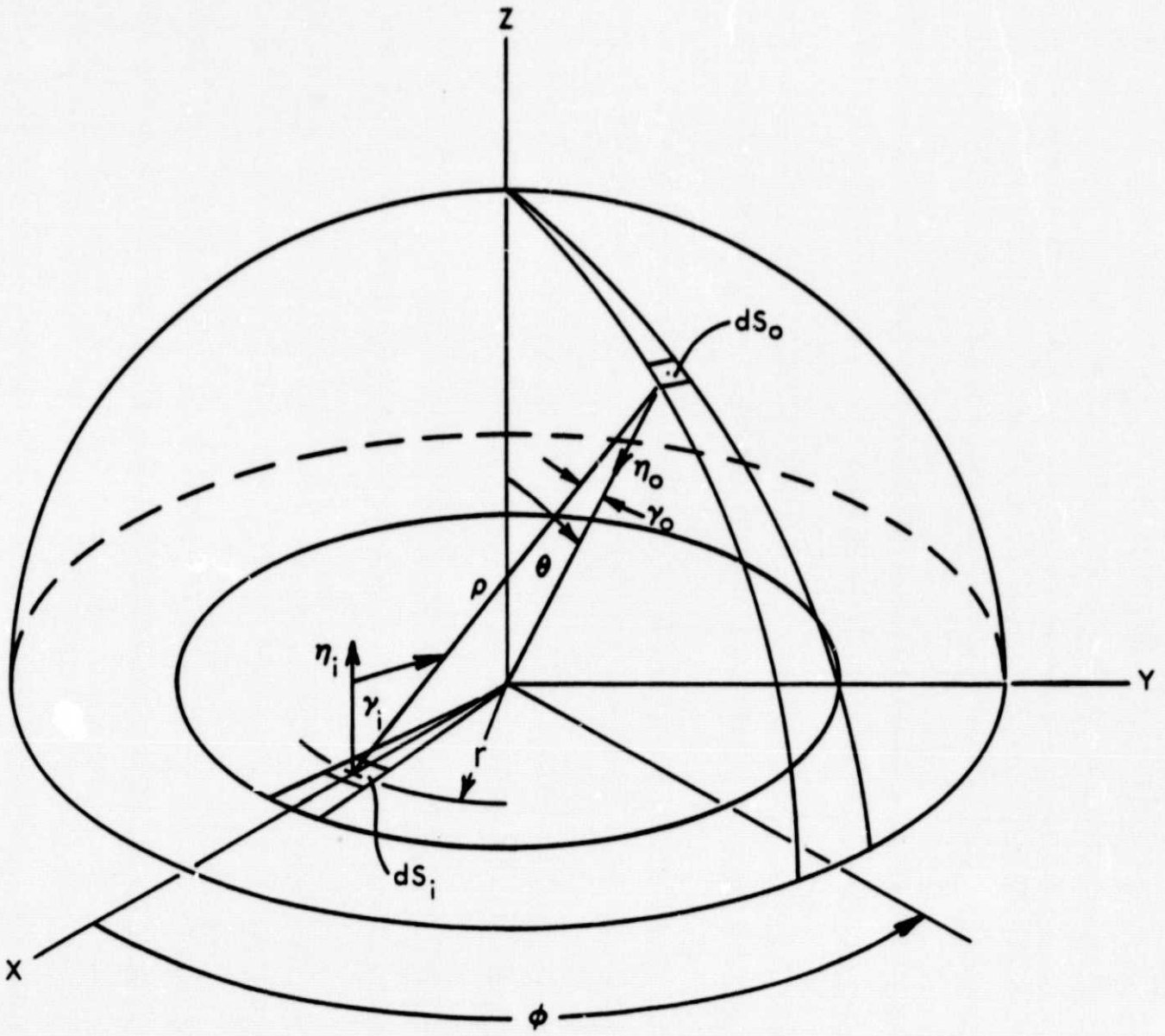

Hemisphere Radius = R_o

Disc Radius = R_i

Normalized Disc Radius = $r/R_o = \nu$

$\nu' = R_i/R_o$

Figure 2. Geometry for the flux density incident on the disc.

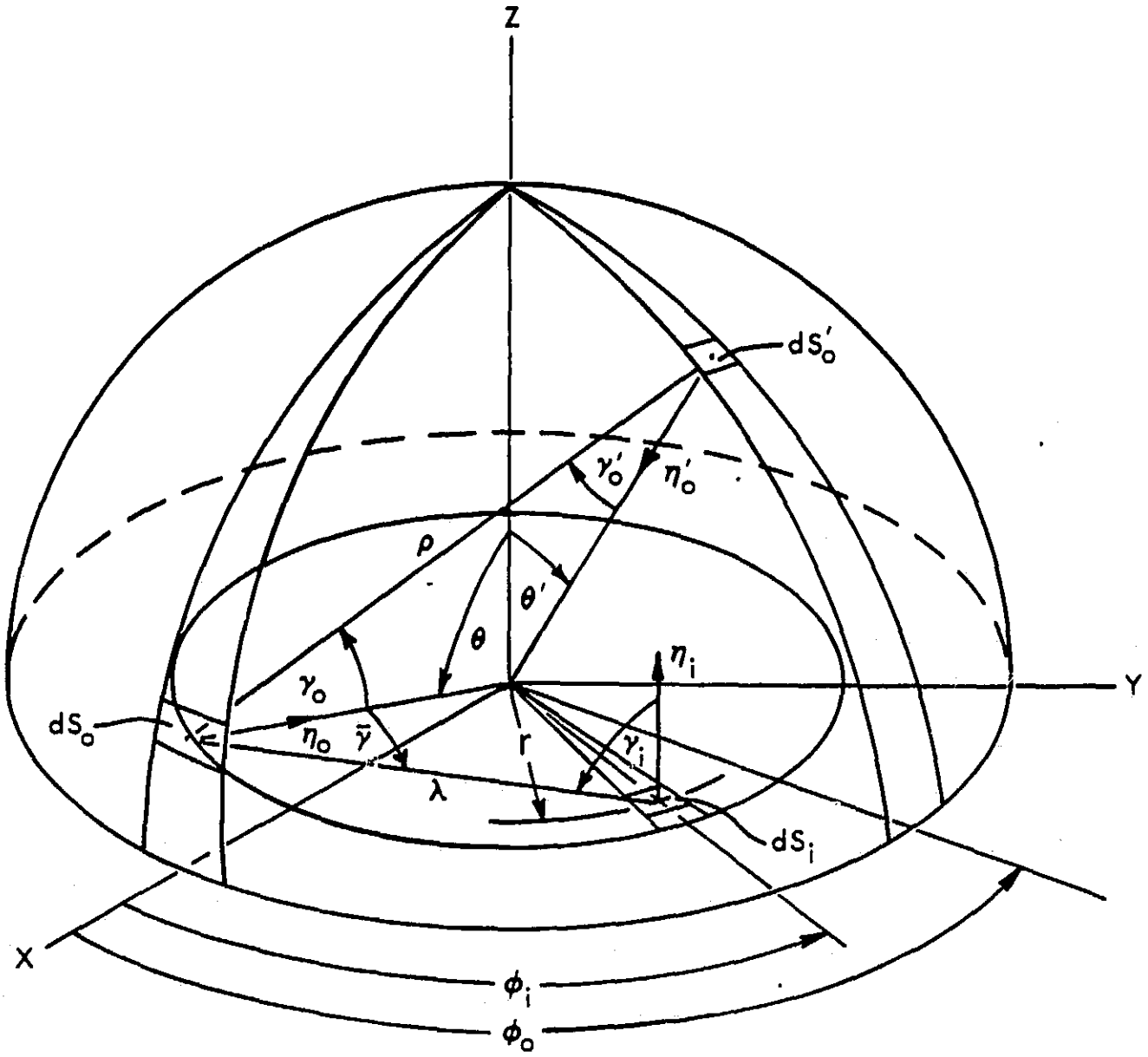

Hemisphere Radius = R_o

Disc Radius = R_i

Normalized Disc Radius = $r / R_o = \nu$

$\nu' = R_i / R_o$

Figure 3. Geometry for the flux density incident on the hemisphere.

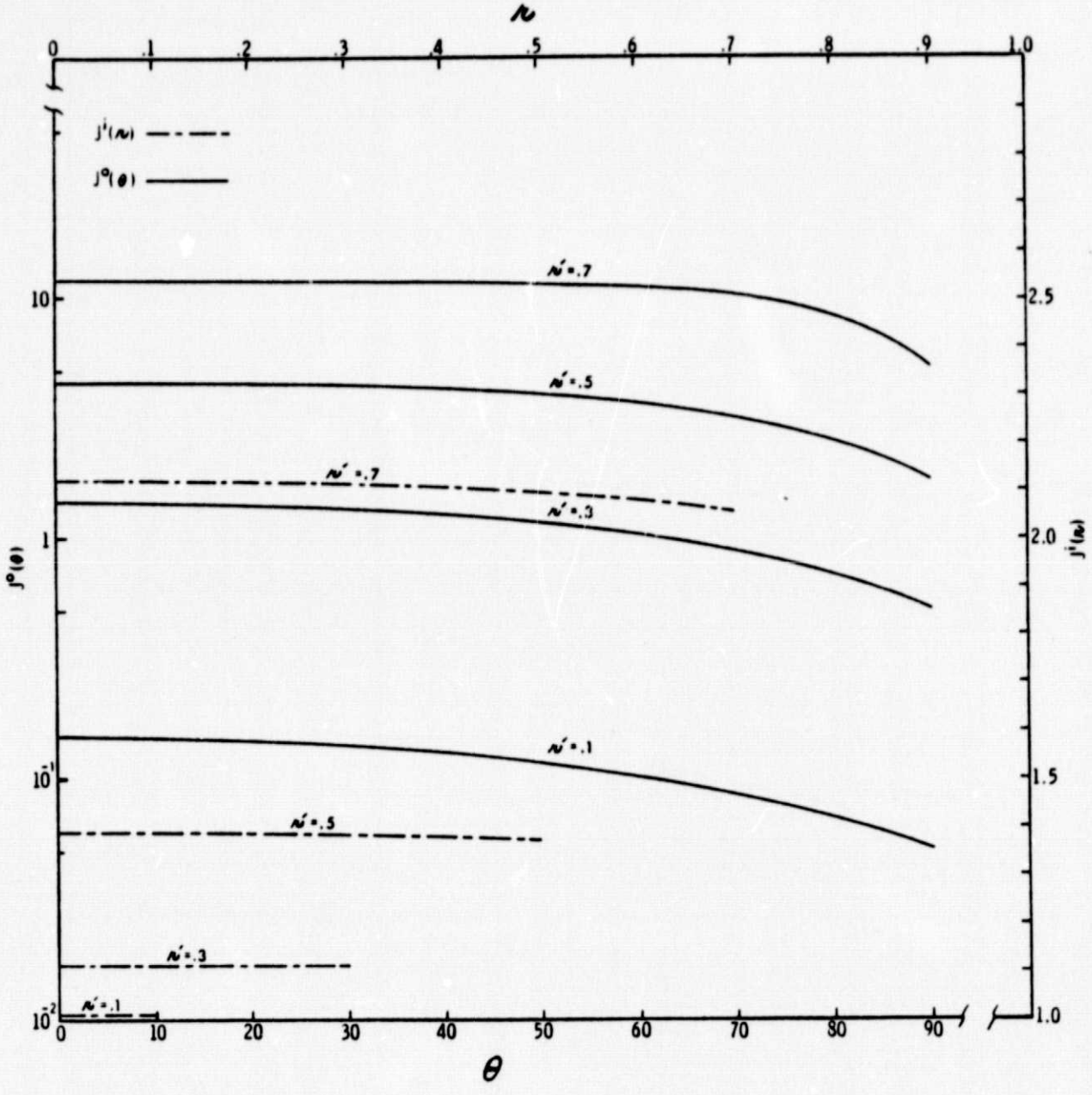

Figure 4. Numerical solutions of the functions $J^{i}(r)$ and $J^{o}(\theta)$ for the system parameter values r' = .1, .3, .5, .7.

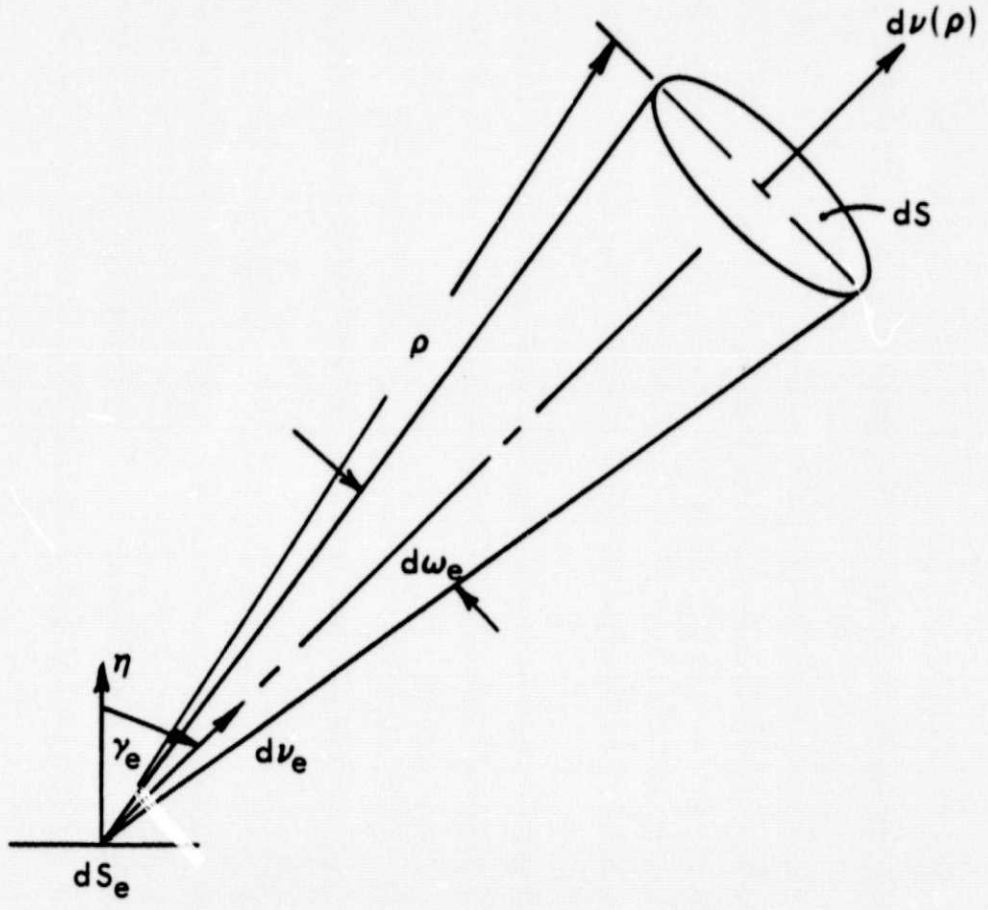

Figure 5. The density at a distance ρ from an emitting surface increment ds_e.

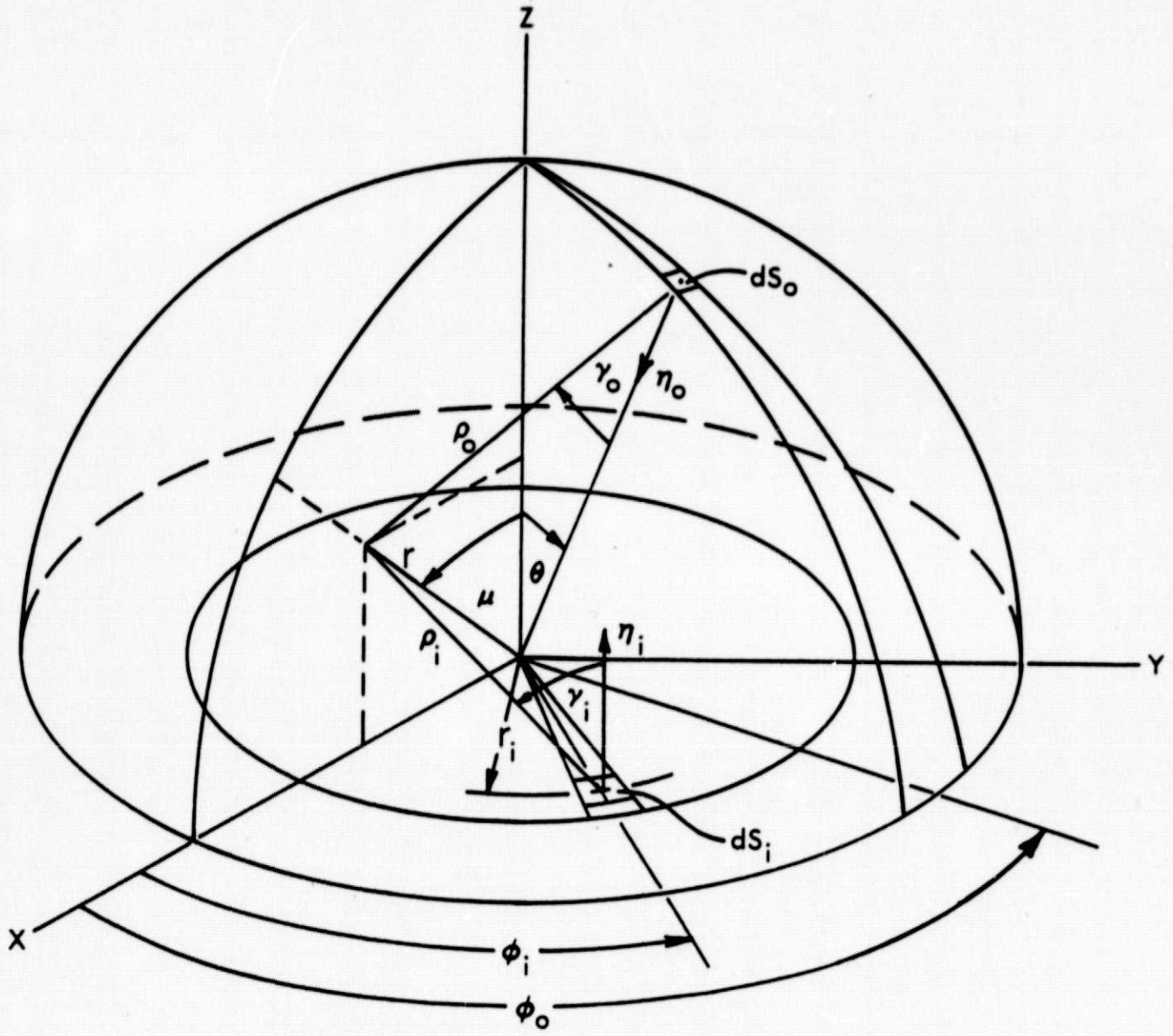

Hemisphere Radius = R_o

Disc Radius = R_i

Normalized Disc Radius = $r_i / R_o = \nu$

Normalized Radius = $r / R_o = \rho$

Figure 6. Model geometry for the density at an arbitrary space point.

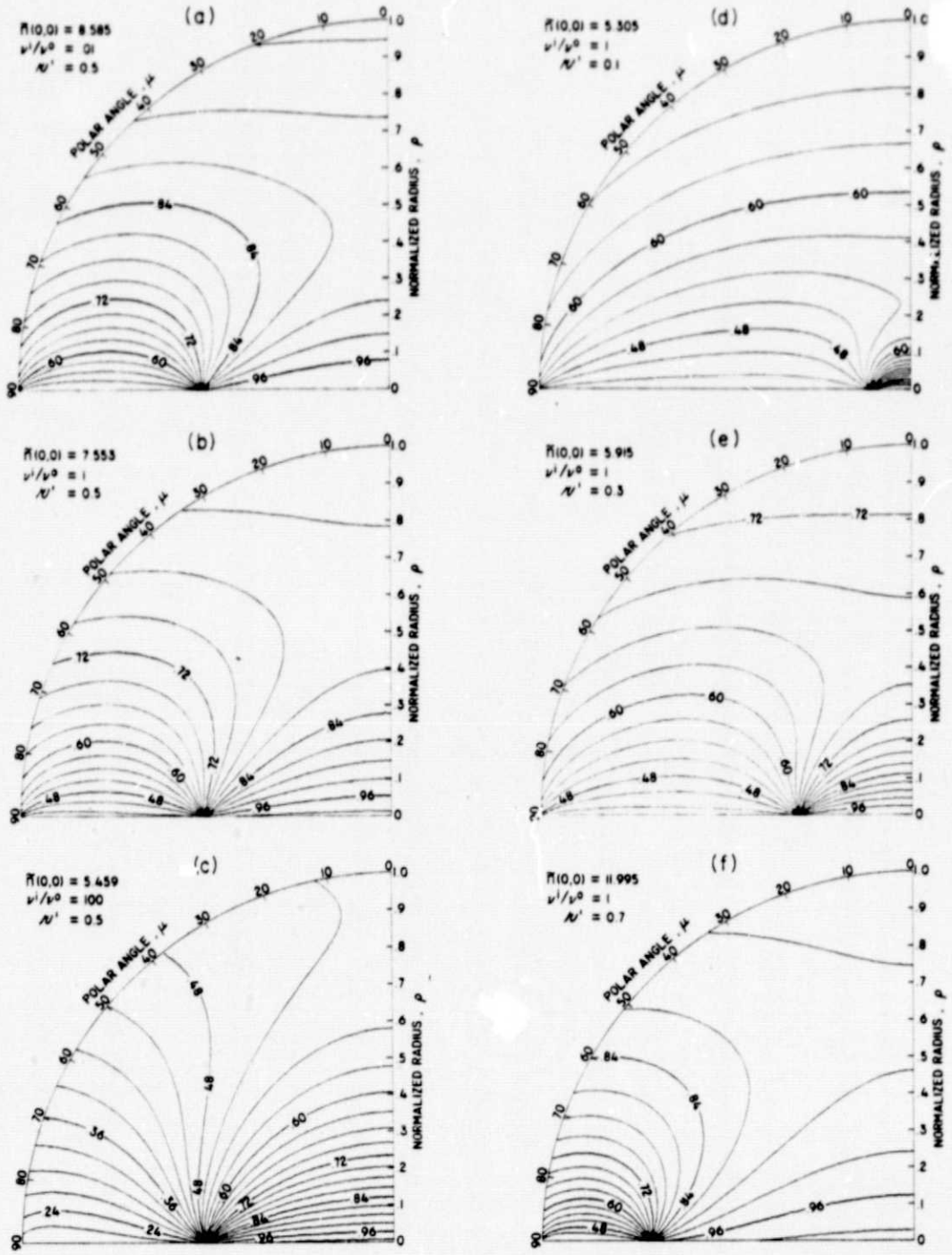

Figure 7. Contours of constant density for the hemisphere-disc system for several values of the system parameters. The contour curves are normalized with respect to the value of the normalized density at the origin $\tilde{n}(0,0)$, which is written on each figure. The density is obtained by inserting the product [contour parameter $\times$ $\tilde{n}(0,0)$] into Eq. (31). The contour parameter interval is 0.03.

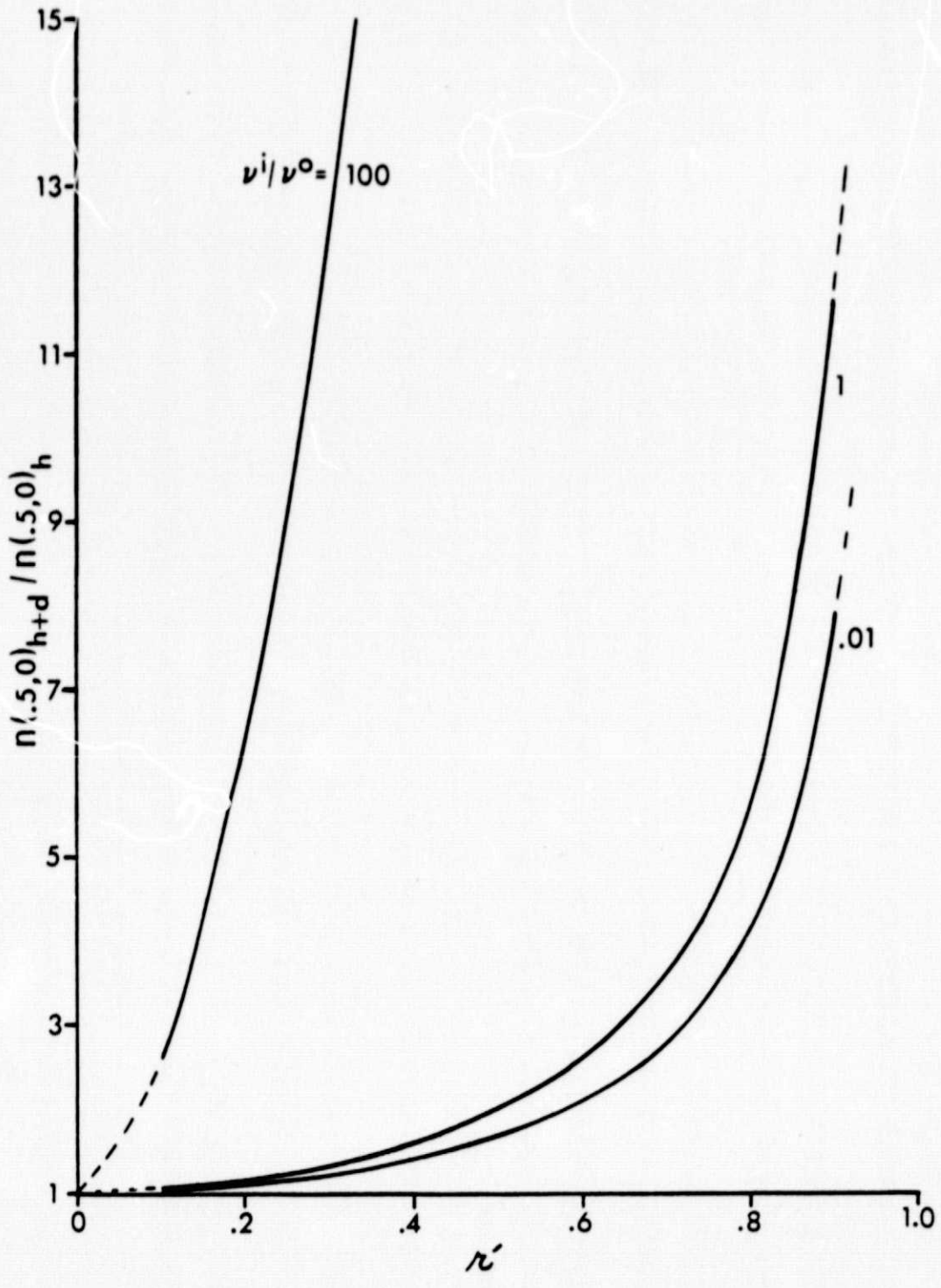

Figure 8. Comparison of the hemisphere-disc system with an empty hemisphere for emission flux density ratios ν^i/ν^o = .01, 1, 100. The ordinate is the density at the center of the hemisphere-disc system $n(1/2, 0)_{h+d}$, divided by the density in the empty hemisphere at the same point $n(1/2, 0)_h$, for the same value of ν^o. The abscissa is the normalized disc radius.

APPENDIX II

DESIGN, DEVELOPMENT, AND EXPERIMENTAL EVALUATION OF QUADRUPOLE MASS SPECTROMETER CIRCUITS

A design for an efficient and accurate emission regulator for the ion source was reported in the literature (see publ. 5). This circuit has been simplified (see fig. 1) to incorporate a different collector power supply and to reduce the parts count of the regulator circuit by eliminating the negative power supply for the op amps. This was made possible by the use of recently introduced CMOS op amps that allow the output to range essentially rail to rail. This circuit has been evaluated while driving a thoria coated iridium cathode in an O_2 atmosphere at various pressures, as shown in table 1. The emission current changed by approximately 0.1 percent as the oxygen pressure ranged from 8×10^{-9} Torr to 5×10^{-4} Torr. The ratio of cathode heater power to bus power to the regulator was better than 0.6.

Two U' voltage generators have been designed--one digital and the other analog. The digital circuit generates a stairstep output where each step can be of preselected height. The analog circuit (see fig. 2) produces a linear ramp with adjustable slope and start-and-stop voltages which may be easily programmed. This design will permit adjustment of the mass range by changing two voltages, rather than requiring a mechanical resetting of a potentiometer.

Work is continuing on the construction of printed circuit versions of the breadboarded circuits, so that a system test can be made. The last major design problem is the RF amplifier to supply the ±V voltages for the quadrupole. This work is being continued under grant NSG 1271.

A portion of the effort under grant NSG 347-003-082 has been spent in the redesign of the ±U amplifier systems occasioned by the appearance on the market of chopper stabilized integrated circuit op amps. Figure 3 shows the schematic of the ±U amplifier circuit. IC_1 and IC_3 are precision chopper stabilized op amps. The combination of IC_1 and Q_1 produces a high voltage, non-inverting op amp with gain controlled by the 6.8 meg resistor and the 220 K resistor in the negative feedback loop. Similarly, IC_2 and Q_2 are connected as a high voltage op amp in the inverting mode. Thus, a single positive going input signal U' drives both +U and -U amplifiers. This drive, U', can be either a linear ramp or a stairstep function. IC_3 is an

error sense amplifier that detects any difference between the +U and -U outputs and feeds the amplified error back to the input of IC_2 in the proper phase to cancel the difference between +U and -U. The trim adjustments allow the following operating modes:

(1) $|-U| = |+U|$

(2) $|-U| = |(+U) + k_1|$

(3) $|-U| = |+U(1 + k_2)|$

where k_1 is a selected fixed offset voltage and k_2 is a selected constant that produces a proportional offset. If the mechanical alignment of the quadrupole rods is ideal, then mode (1) would be used.

Table 2 shows the performance of the circuit using carbon resistors in the feedback loop. The outputs are highly symmetrical, i.e., track each other; however, they do not track the input at high voltages, the departure from linearity being almost five percent. This effect is due to the fact that carbon resistors have an R = f(V) characteristic that is non-negligible. Table 3 shows how the substitution of metal film precision resistors in the critical feedback circuits eliminates the effect. The ±U outputs not only track each other with low error (< 0.1 percent) but the outputs now track the input with an error of < 0.1 percent, an improvement of a factor of 50. (See table 1 and table 2.)

Figure 4 and figure 5 show the x-y plotter output for the +U and -U amplifiers, when driven by a linear ramp function. The circuit has been tested using a stairstep function to determine that the op amp output settling time was consistent with the design requirements.

The design of an electron multiplier and ion counting circuits were not worked out during this reporting period and will be addressed in a subsequent grant.

Table 1. Emission control circuit using single ended power supply. Performance vs. O_2 pressure.

$V_{supply\ Bus}$ Volts	$I_{supply\ Bus}$ ma	Emission Current, $I_{\mu amp}$	Pressure O_2 Torr	$V_{collector}$ Volts	Power from Bus Watts
28.0	61.0	100.28	8.2×10^{-9}	59.0	1.71
28.0	61.5	100.28	5×10^{-8}	59.0	1.72
28.0	64.2	100.27	5×10^{-7}	59.1	1.80
28.0	70.4	100.28	5×10^{-6}	59.1	1.97
28.0	76.2	100.30	5×10^{-5}	59.2	2.13
28.0	82.0	100.4	5×10^{-4}	59.2	2.30

Table 2. ±U amplifier performance with carbon 6.8 meg ohm resistors in feedback divider circuit.

U' (v)	U^+ (v)	U^- (v)	% Diff.	Gain
0.05005	1.662	1.655	-0.181	33.207
0.10091	3.351	3.354	-0.089	33.208
0.14937	4.961	4.965	-0.081	33.213
0.2002	6.649	6.653	-0.068	33.209
0.2998	9.958	9.964	-0.060	33.215
0.3997	13.273	13.281	-0.061	33.206
0.5007	16.613	16.622	-0.054	33.179
0.6995	23.201	23.211	-0.043	33.168
1.0016	33.192	33.205	-0.038	33.139
1.5006	49.636	49.655	-0.038	33.077
2.003	66.100	66.166	-0.024	33.000
2.502	82.359	82.374	-0.018	32.917
3.001	98.454	98.465	-0.011	32.807
3.503	114.551	114.559	-0.007	32.700
4.002	130.419	130.420	-0.0008	32.588
4.501	146.297	146.292	0.003	32.503
5.001	161.962	161.949	0.008	32.386
5.500	177.462	177.449	0.007	32.266
6.000	192.864	192.843	0.011	32.144
6.500	208.14	208.10	0.019	32.022
7.002	223.29	223.23	0.027	31.889
7.502	238.32	238.27	0.021	31.767
8.002	253.24	253.19	0.020	31.647
8.201	259.13	259.08	0.019	31.597

Maximum difference between $U^+ - U^-$ = 0.181%.

Maximum change in gain = 4.87%.

Table 3. ±U amplifier performance with film 6.8 meg ohm resistors in feedback divider circuit.

U' (v)	U^+ (v)	U^- (v)	% Diff.	Gain
0.05000	1.581	1.582	-0.063	31.620
0.10087	3.191	3.192	-0.031	31.635
0.15044	4.759	4.760	-0.021	31.634
0.2000	6.329	6.330	-0.016	31.645
0.2520	7.973	7.973	--	31.639
0.3006	9.514	9.514	--	31.650
0.4000	12.656	12.656	--	31.640
0.5012	15.860	15.860	--	31.644
1.0001	31.649	31.649	--	31.646
1.5016	47.519	47.519	--	31.646
2.001	63.328	63.328	--	31.648
2.500	79.118	79.118	--	31.647
3.003	95.024	95.024	--	31.643
3.502	110.818	110.818	--	31.644
4.002	126.644	126.644	--	31.645
4.503	142.501	142.501	--	31.646
5.000	158.223	158.223	--	31.645
5.501	174.103	174.103	--	31.649
6.001	189.944	189.944	--	31.652
6.501	205.73	205.71	+0.0097	31.646
7.000	221.54	221.52	0.0090	31.649
7.501	237.39	237.36	0.0126	31.648
8.005	253.34	253.31	0.0118	31.648
8.197	259.42	259.39	0.0116	31.648

Maximum difference between $U^+ - U^-$ = 0.063%.

Maximum change in gain = 0.095%.

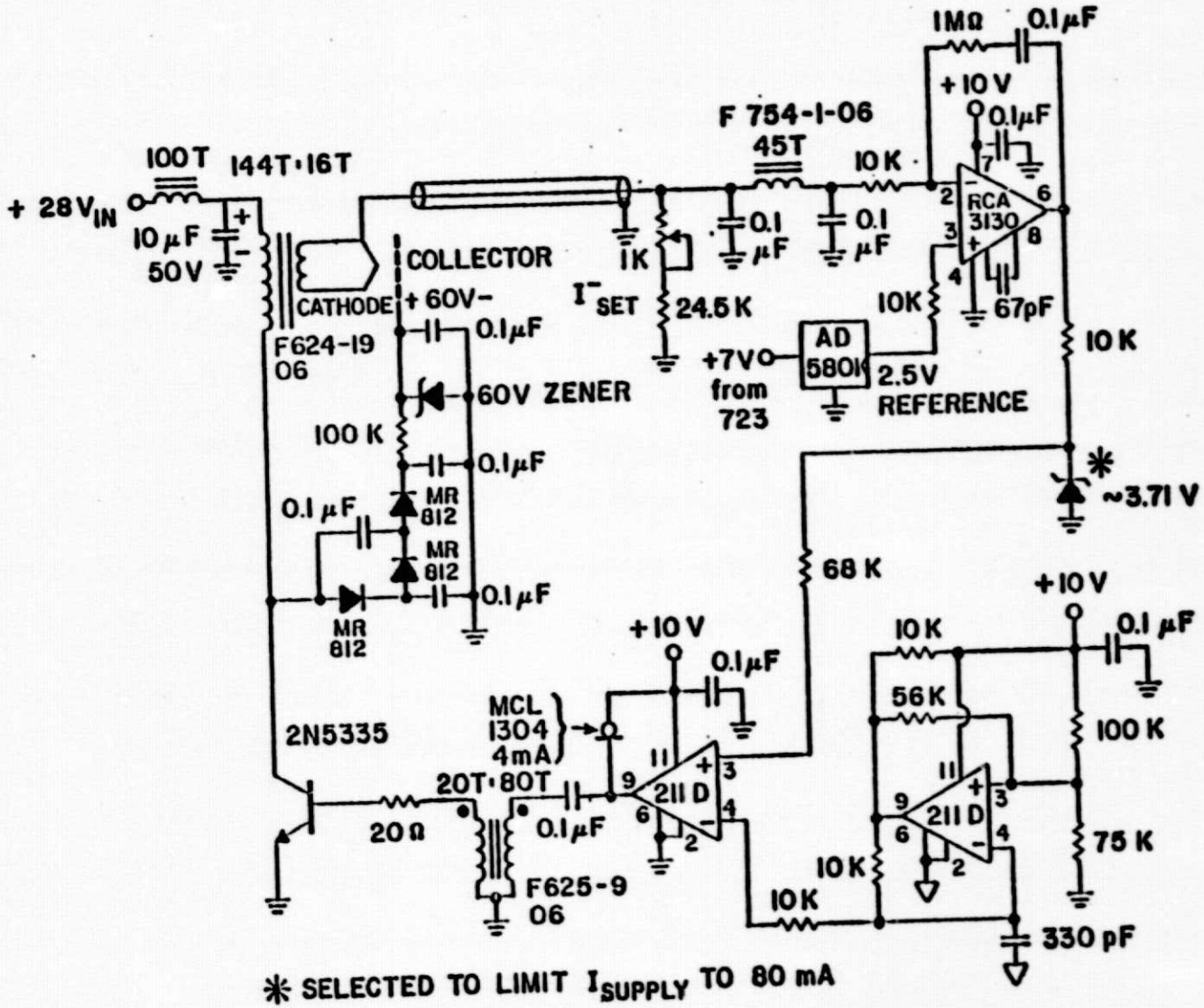

Figure 1. Emission regulator.

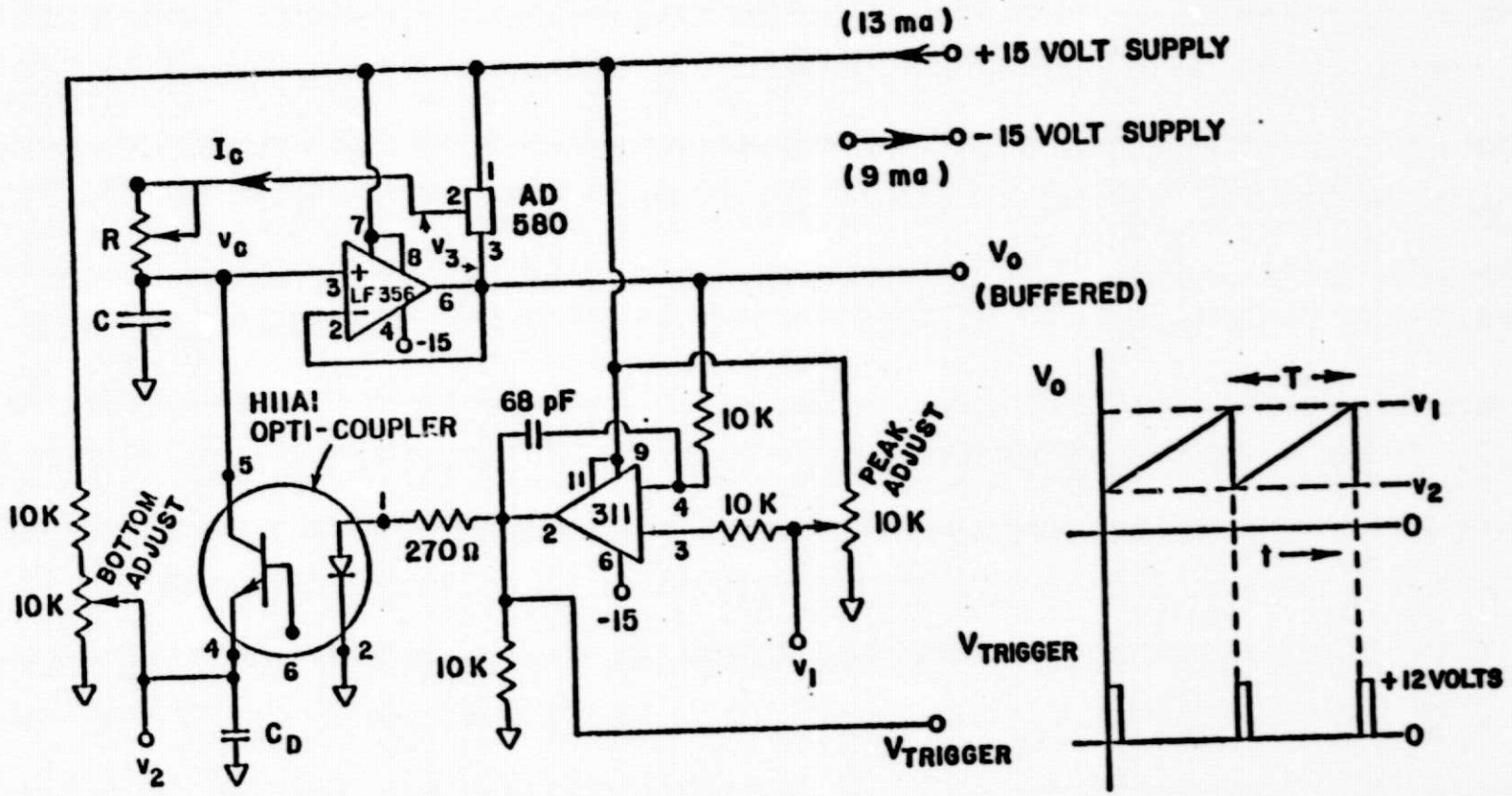

NOTES:

(1) VALUE OF R DETERMINES SLOPE OR $\frac{dV_O}{dt}$

(2) $T = RC\left[\frac{V_1 - V_2}{V_3}\right]$

(3) $C_D > 100C$

(4) $I_C = \frac{V_3}{R}$

Figure 2. Linear ramp generator with buffered output, separately adjustable slope, and peak and bottom voltage.

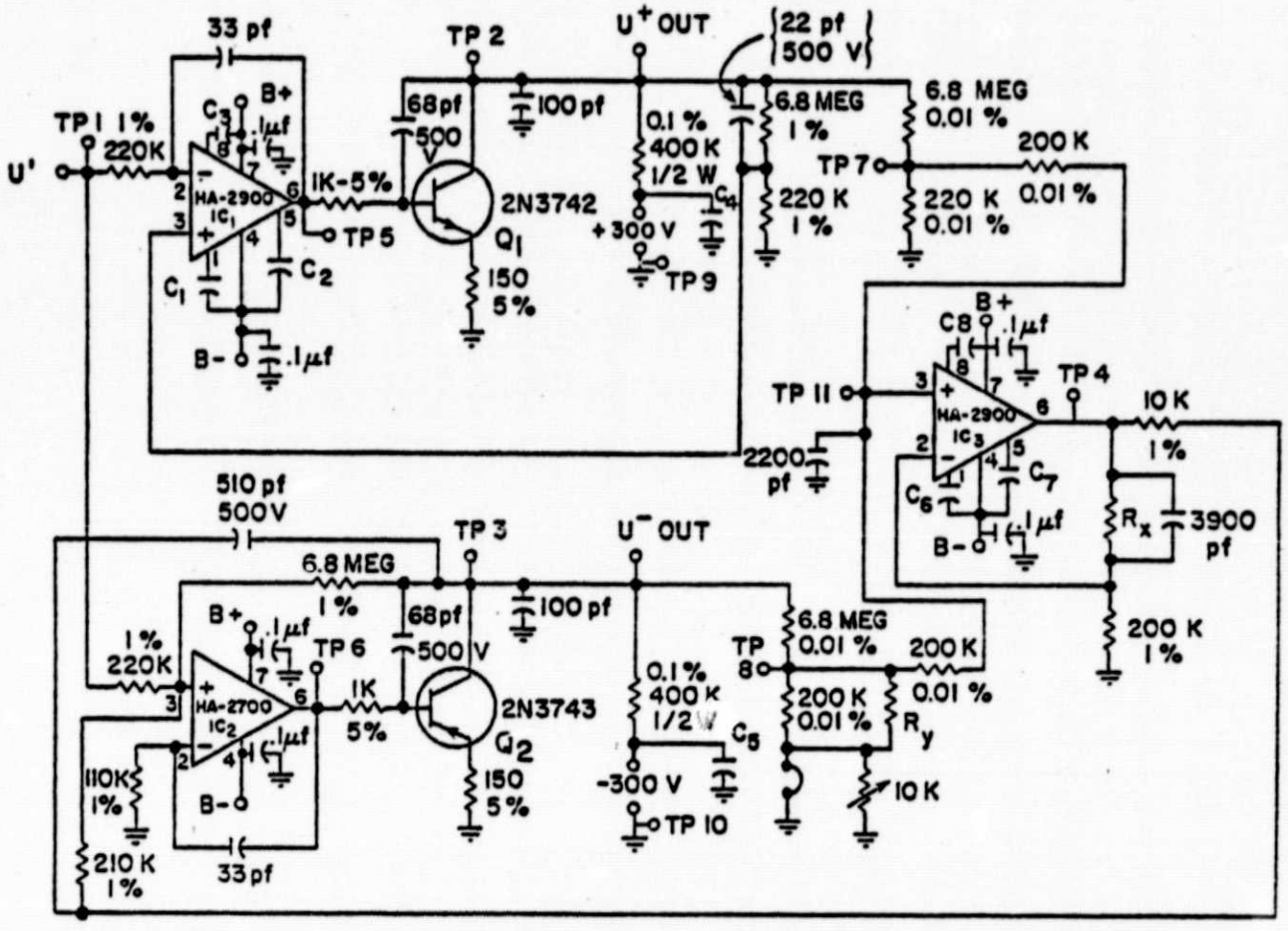

C_1, C_2, C_6, C_7 — 0.1μf, 100 V POLYCARBONATE (0.5" x 1.125")
C_3, C_8 — 1500 pf SILVER MICA
C_4, C_5 — 0.01μf, 500 V CERAMIC
R_x — TO BE DETERMINED IN TRIM PROCEDURE
R_y — TO BE DETERMINED IN TRIM PROCEDURE

Figure 3. U amplifier.

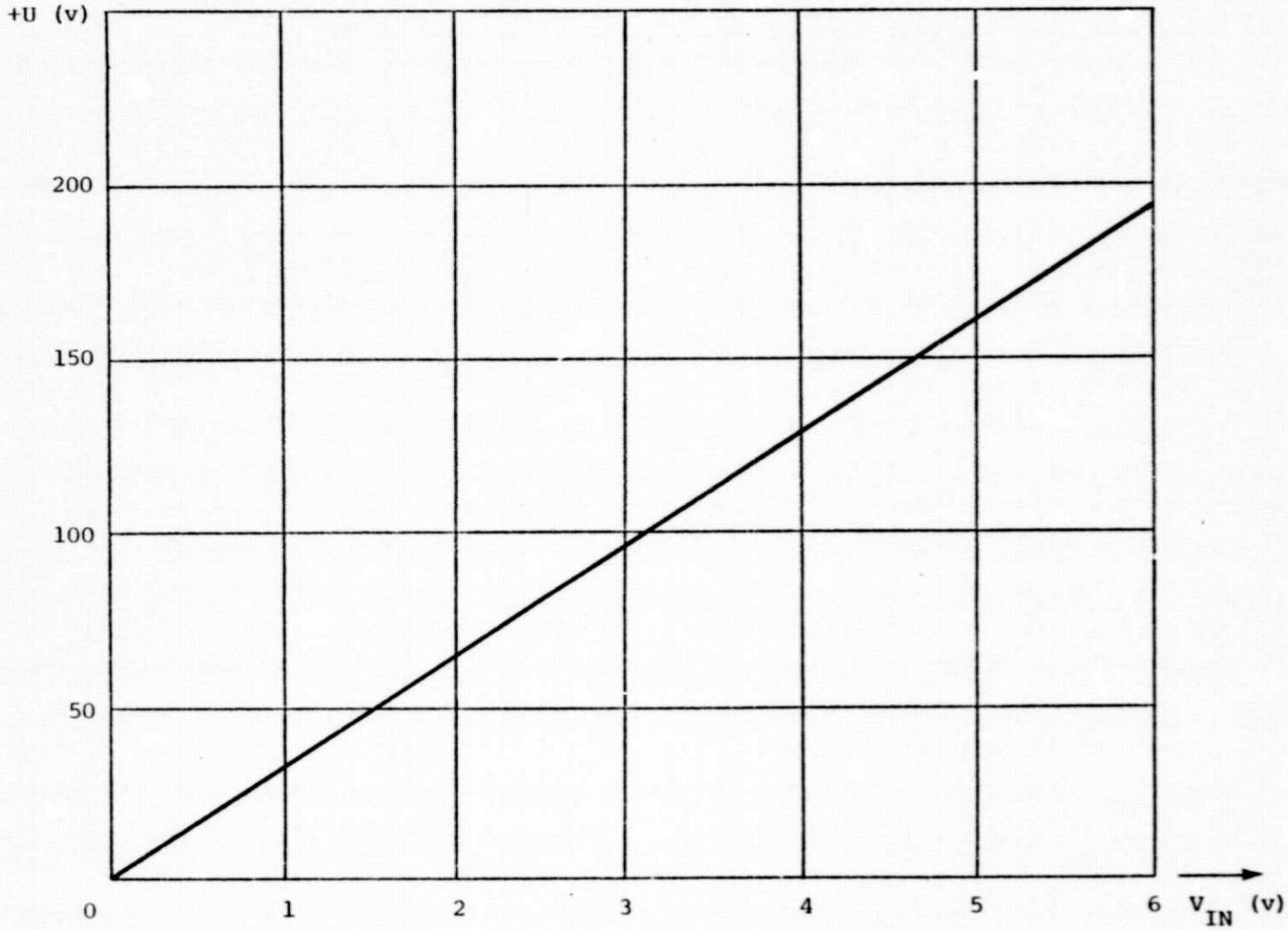

Figure 4. +U amplifier performance. (x-y plotter output).

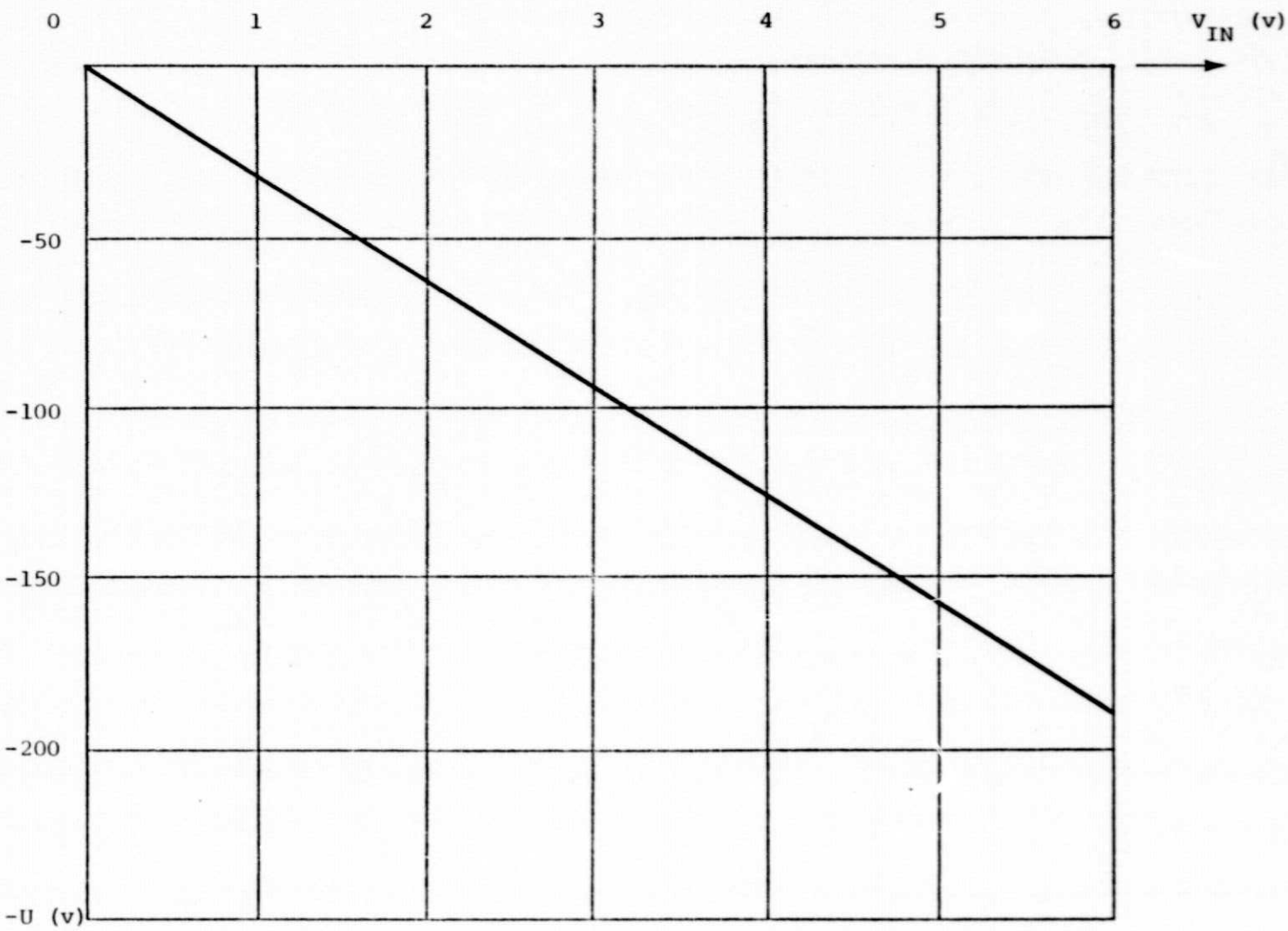

Figure 5. -U amplifier performance. (x-y plotter output).